Organic Composition of C/1999 S4 (LINEAR): A Comet Formed Near Jupiter?

M. J. Mumma,[1]* N. Dello Russo,[1,2] M. A. DiSanti,[1,2]
K. Magee-Sauer,[3] R. E. Novak,[4] S. Brittain,[5] T. Rettig,[5]
I. S. McLean,[6] D. C. Reuter,[1] Li-H. Xu[7]

In the current paradigm, Oort cloud comets formed in the giant planets' region of the solar nebula, where temperatures and other conditions varied greatly. The measured compositions of four such comets (Halley, Hyakutake, Hale-Bopp, and Lee) are consistent with formation from interstellar ices in the cold nebular region beyond Uranus. The composition of comet C/1999 S4 (LINEAR) differs greatly, which suggests that its ices condensed from processed nebular gas, probably in the Jupiter-Saturn region. Its unusual organic composition may require reevaluation of the prebiotic organic material delivered to the young Earth by comets.

Measuring the composition of cometary nuclei is key to understanding the formation and evolution of matter within the early solar system (*1*, *2*). In the current paradigm, the so-called Oort cloud (OC) comets (*3*) formed in the giant planets' region of the solar nebula [an area extending from 5 to 40 astronomical units (AU) from the Sun]. During this formation period, nebular temperatures (*4*) ranged from about 200 K near Jupiter (~5 AU) to about 30 K near Neptune (~40 AU), and other conditions also varied. Each of the four giant planets scattered about the same number of comets into the Oort cloud (*5*)—the reservoir for this dynamical group—so chemical differences might appear among even a small sample of them (*6–11*).

The ices in OC comets Halley, Hyakutake, and Hale-Bopp (*12*) revealed compositions similar to those in dense interstellar cloud cores (*7*, *13–15*). The observed deuterium enrichment (*16*), the low ortho-para ratios displayed by water (*17–19*), and the depletion of neon (*20*, *21*) with a possible enhancement of argon (*22*) all support processing at temperatures near 30 K. This suggests the accumulation of precometary ices in the Uranus-Neptune region, where the great

distance from the Sun and the large amount of intervening nebular material may have offered protection against extensive thermal and radiation processing. The symmetric hydrocarbons (methane, acetylene, and ethane) and methanol were comparably abundant in these three comets and in OC comet Lee (*10*), which is consistent with a common origin, but native CO varied sixfold among them: perhaps a signature of slightly different formation temperatures.

Comet C/1999 S4 (LINEAR) (C/LINEAR) was discovered on 27 September 1999 by the Lincoln Near Earth Asteroid Research (LINEAR) program (*23*), while still at 4.2 AU from the Sun (1 AU = the mean Earth-Sun distance). Subsequent observations revealed it to be an OC comet, probably reentering the inner solar system for the first time (*24*), and orbital predictions suggested that it would become a favorable target for observations during July 2000, when it would be close to Earth (~0.4 AU) and to the Sun (~0.8 AU). Such conditions favor the infrared (IR) detection of parent volatiles, such as were obtained for comets Hyakutake (*25–27*), Hale-Bopp (*9*, *28–30*), and Lee (*10*). We report similar detections in C/LINEAR before its final breakup in late July.

The organic volatile composition of C/LINEAR was investigated by high-dispersion IR spectroscopy (in the wavelength range from 2.0 to 4.7 μm) using cryogenic echelle grating spectrometers at the NASA Infrared Telescope Facility (IRTF) (*31*, *32*) and at the W. M. Keck Observatory (*33*, *34*), both located on Mauna Kea, Hawaii (Table 1). These spectrometers provide long-slit spectra with high spatial resolution about the cometary nucleus (*35*). We followed our standard procedures for acquisition of cometary (*36*) and stellar (*37*) spectra and for data reduction (*38*) and analysis. Cometary

molecular emissions were isolated by subtracting a modeled dust continuum convolved with the synthesized atmospheric transmittance (*39*).

Water (H_2O), methane (CH_4), carbon monoxide (CO), and hydroxyl (OH) were detected with the cryogenic echelle spectrometer (CSHELL) (Fig. 1 and Table 2). Ethane (C_2H_6), hydrogen cyanide (HCN), H_2O, CH_4, NH_2, and OH were detected with the near-infrared echelle spectrometer (NIRSPEC), and stringent upper limits were set for methanol (CH_3OH) and acetylene (C_2H_2) (Fig. 2 and Table 2). Selected NIRSPEC spectral orders are compared with those of comet Lee and with the modeled continuum emission from cometary dust (as extinguished by the terrestrial atmosphere) in Fig. 2. The atmospheric water content was unusually high on 13 July [~7.3 precipitable millimeters (pr-mm)], so the transmittance in some spectral regions was much less favorable than when comet Lee was observed (~1 pr-mm). This effect is explicitly included in our reductions. Molecular column densities were obtained from measured line intensities using an excitation model, after correcting for atmospheric transmittance at the Doppler-shifted position of each cometary line. When a sufficient number of lines is detected, the integrated band emission intensity may be obtained from the measured line intensities using solar fluorescence efficiencies (*g* factors) appropriate to the derived rotational temperature (*40–43*). In comets Hyakutake, Hale-Bopp, and Lee, a single temperature characterized the rotational distribution of different species when measured under common conditions. For C/LINEAR, too few lines were detected to permit independent determination of a rotational temperature, so we adopted a temperature (50 K) typical of other comets of similar activity and heliocentric distance (*44*). We extracted apparent production rates (*Q*) using *g* factors (*9*, *10*, *29*, *30*, *45*, *46*) appropriate to this temperature and assuming spherically symmetric outflow from the nucleus at a uniform velocity (0.8 km s^{-1}) (*47*).

OH prompt emission (Fig. 2) serves as a proxy for its parent species (H_2O) (*48–52*). Because it tracks the production rate and spatial distribution of water, we use OH prompt emission to compare the activity of the comet on various dates and to tie the production rates of other species to a common reference (Table 2). The production efficiency of the OH quadruplet ($v' = 1$, $J' = 10.5, 11.5$) near 3046 cm^{-1} (Fig. 2C) was calibrated against the H_2O production rate measured for comet Lee (*10*). In C/LINEAR, one line of this multiplet was detected on 5 July (Fig. 1C), whereas three lines were detected on 13 July (the fourth was obscured by atmospheric water, which was unusually abundant on that date) (Fig. 2C). We correct-

[1]Laboratory for Extraterrestrial Physics, Code 690, NASA Goddard Space Flight Center, Greenbelt, MD 20771, USA. [2]Department of Physics, The Catholic University of America, Washington, DC 20064, USA. [3]Department of Chemistry and Physics, Rowan University, Glassboro, NJ 08028, USA. [4]Department of Physics, Iona College, New Rochelle, NY 10801, USA. [5]Department of Physics and Astronomy, University of Notre Dame, Notre Dame, IN 46556, USA. [6]Department of Physics and Astronomy, University of California, Los Angeles, Los Angeles, CA 90095–1562, USA. [7]Department of Physical Sciences, University of New Brunswick, Saint John, New Brunswick, Canada E2L 4L5.

*To whom correspondence should be addressed. E-mail: mmumma@kuiper.gsfc.nasa.gov

ed the multiplet *g* factor to account for only the lines seen in C/LINEAR, and we obtained a measure of the water production rate (Table 2). Production rates based on a water line and OH prompt emission are in reasonable agreement on 5 July, demonstrating the internal consistency of our results. Two lines of the OH quadruplet near 2996 cm^{-1} were similarly calibrated and were used to obtain a water production rate on 9.6 July (Table 2).

Methanol was not detected in C/LINEAR (Fig. 2A); its relative abundance (*53–56*) (Table 2) is at least a factor of 10 lower than that found for comet Lee (*10*). Ethane and methane were detected in C/LINEAR but at low levels as compared with the four comparison OC comets. Three *Q* branches of the C_2H_6 ν_7 band were seen on 13 July (Fig. 2B), and upper limits for C_2H_6 were obtained (*57*) on 4, 5, and 9 July (Table 2). The strongest emission lines of the CH_4 ν_3 band (R0 and R1) were expected to appear in order 23 of setting KL2 (Table 1 and Fig. 2C), along with weaker lines (P2 and P3) in order 23 of setting KL1 (Fig. 2B). We detected R0, R1, and P2 in C/LINEAR. OH prompt emission lines were the strongest lines seen (Fig. 1C and Fig. 2, A through D). The weakness of the CH_4 and C_2H_6 lines relative to OH prompt emission graphically indicates the depletion of methane and ethane relative to water in this comet, as compared with comet Lee. The high atmospheric water burden on 13.8 July severely affected atmospheric transmittance near 3300 to 3330 cm^{-1}, reducing the number of HCN and C_2H_2 lines eligible for detection (Fig. 2D). Nevertheless, HCN was detected and a stringent upper limit was obtained for C_2H_2 (Table 2). Acetylene is a possible parent of C_2, and C/LINEAR is depleted in C_2 (*58*).

Production rates (or upper limits) are given for seven parent volatile species in C/LINEAR (Table 2); we take these to represent the abundances of ices in the nucleus. Our production rates generally agree with those obtained with other approaches, when measured on common dates. For example, our production rate for CO on 5.8 July ($7 \pm 2 \times 10^{26}$ molecules s^{-1}) agrees with that derived from simultaneous Hubble Space Telescope (HST) observations ($\sim 5 \times 10^{26}$ molecules s^{-1}) (*59*). Our (2σ) upper limit for CH_3OH ($< 0.17\%$ of H_2O) is more restrictive than the upper limit obtained from millimeter spectra (*60*). Our H_2O production rate on 5.8 July is intermediate to our retrieval for 4.6 July and to HST retrievals for 6.8 July, suggesting a rapid and continuing increase in H_2O production over those dates (*61*, *62*). The mixing ratios of trace species measured on 5.8 July agree with measurements on 13.6 July, suggesting that the outburst of 5 to 7 July was not driven by an unusually high release of highly volatile species such as CH_4, C_2H_6,

or CO. The most volatile species are highly depleted in C/LINEAR, suggesting that mechanisms other than their sudden release must be sought for explaining its complete disruption. If the nucleus was a weakly bound small clump of cometesimals, dissipation of ices at the interfaces between cometesimals would progressively lessen the adhesive forces binding them to one another, permitting rotational shedding (*63*) and ultimately complete disruption.

The relative abundances of most trace species in C/LINEAR are smaller than those in the other four OC comets by factors of 5 to 10 (Table 2). The abundance of (native) CO in C/LINEAR ($0.9 \pm 0.3\%$) is much lower than in comets Lee ($1.8 \pm 0.2\%$) (*10*), Halley (3.5%) (*64*), Hyakutake (~ 10 to 14%) (*65*), and Hale-Bopp ($12.3 \pm 0.7\%$) (*9*). CH_4 and C_2H_6 are less abundant by about a factor of 6 in C/LINEAR, and C_2H_2 is smaller by at least a factor of 2.5 as compared with the other OC
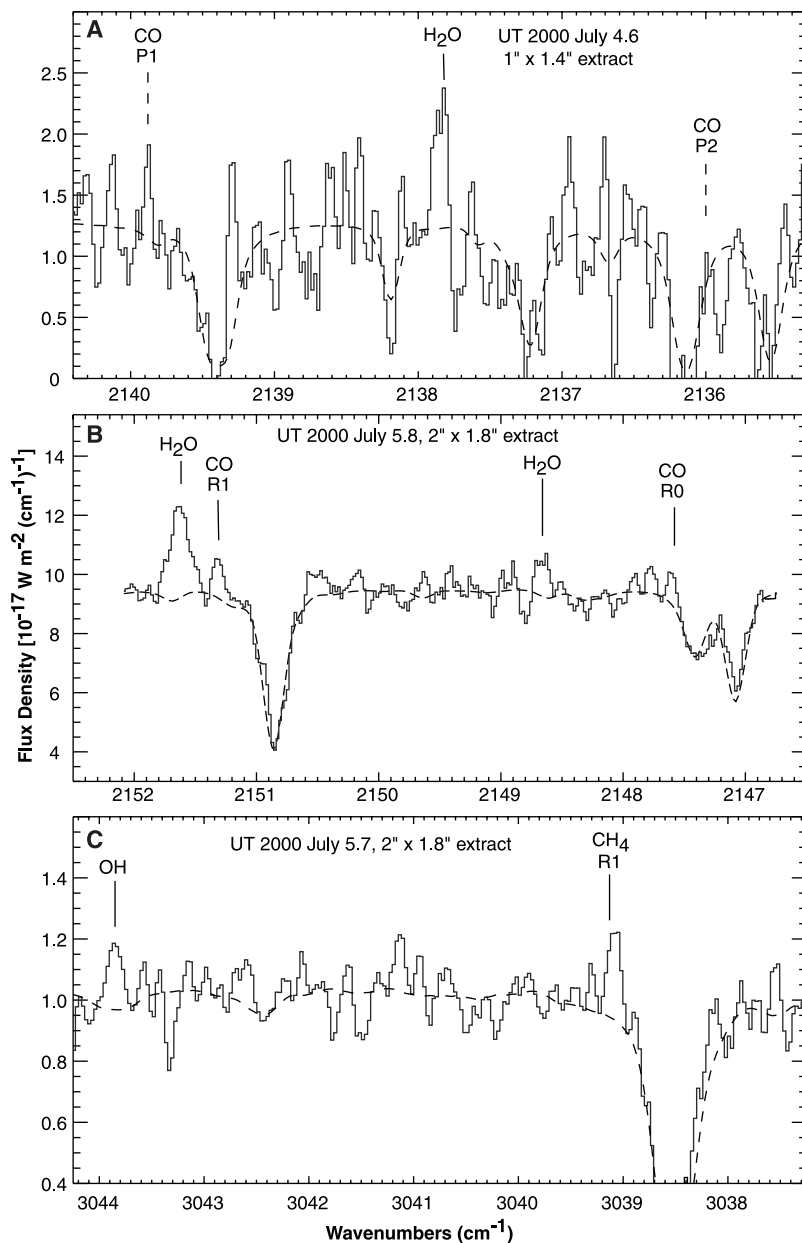

Fig. 1. CSHELL spectra of C/LINEAR. The cometary lines are blue-shifted (by ~ -63 km s^{-1}) relative to their rest frequencies. The modeled atmospheric transmittance (dashed lines) and the observed comet spectra (solid lines) are shown. (**A**) Detection of H_2O on UT 4.6 July. CO line assignments are indicated. The detected water line is part of the (ν_3-ν_2) band, rotational designation 0_{00}-1_{01} (rest frequency, 2137.37 cm^{-1}). (**B**) Detection of CO and H_2O on UT 5.8 July. CO line assignments are indicated. The detected water lines are as follows: (ν_3-ν_2) band, rotational designation 1_{11}-1_{10} (rest frequency, 2151.19 cm^{-1}) and (ν_1-ν_2) band, rotational designation 2_{21}-1_{10} (rest frequency 2148.19 cm^{-1}). (**C**) Detection of CH_4 (ν_3, R1 line) and OH (1-0 band, P12.5 1^-) on UT 5.7 July.

comets (*66*). These depletions could reflect condensation at moderately high nebular temperatures (*67, 68*), or preferential loss from interstellar ices as a result of thermal processing. CH_4, C_2H_6, and C_2H_2 are apolar species, and CO has a relatively small dipole moment (*69*) [$\mu = 0.11$ debye (D)]. Thus, their ices are more volatile than hydrogen-bonded ices

of polar species [such as H_2S, CH_3OH, H_2O, H_2CO, and HCN, for which $\mu = 0.97$, 1.70, 1.85, 2.33, and 2.98 D, respectively (*69*)]. Thermal processing should cause the more volatile species to be depleted by factors related to their surface bonding strengths. CO and CH_4 should show the largest depletions, followed by C_2H_6 and then C_2H_2. However,

the hydrogen-bonded species should not be as strongly depleted.

Among the less volatile ices, H_2S and H_2CO are present in normal abundance relative to HCN (*60*). Our simultaneous measurements of H_2O and HCN on 13.8 July suggest that HCN is depleted by about a factor of 2 relative to H_2O, when compared with comet

Fig. 2. NIRSPEC spectra of C/LINEAR (lower trace in all panels) on UT 13.6 July. Selected high-dispersion spectra (RP ~15,000) of C/LINEAR are compared with those of comet Lee (*10*) (upper trace in all panels). The spectra are normalized so that OH emission lines have the same intensity in comets Lee and C/LINEAR. The lines are Doppler-shifted relative to their terrestrial counterparts, owing to the comet's geocentric motion (by ~ −29 km s⁻¹ in comet Lee and −55 km s⁻¹ in C/LINEAR). Synthetic spectra of the atmospheric transmittance do not line up, because the spectra are shown in the cometary rest frames. The unusually high atmospheric water abundance severely affected transparency during observations of C/LINEAR. In all panels, ? indicates emission lines from unidentified species. (**A**) Setting KL1, order 22: methanol ν_3 region. The triply peaked Q branch is prominent in comet Lee, and many lines in the P and R branches are also detected. OH lines (§) (1-0 band) and possibly H_2CO (o) are detected in C/LINEAR, but no CH_3OH (‡) emission is seen. (**B**) Setting KL1, order 23: ethane ν_7 region. The marked lines in comet Lee are identified as follows (reading from higher wavenumber to lower). #: C_2H_6, ν_7, $^RQ_4$, $^RQ_3$, $^RQ_1$, $^RQ_0$, $^PQ_1$, $^PQ_3$, and $^PQ_4$; ◇: CH_4, ν_3, P2, and P3; ‡: CH_3OH, ν_2, and ν_9; §: OH (1-0) (P12.5 2⁺ and 2⁻, P13.5 1⁺ and 1⁻). In C/LINEAR, only selected lines are seen. C_2H_6, ν_7, $^RQ_1$, $^PQ_1$, and $^PQ_3$; CH_4, ν_3, P2; OH (1 to 0) (P13.5 1⁺ and 1⁻). (**C**) Setting KL2, order 23: methane ν_3 region. §: OH (1 to 0) (P11.5 2⁺ and 2⁻, P12.5 1⁺ and 1⁻); and ◇: CH_4, ν_3, R1, and
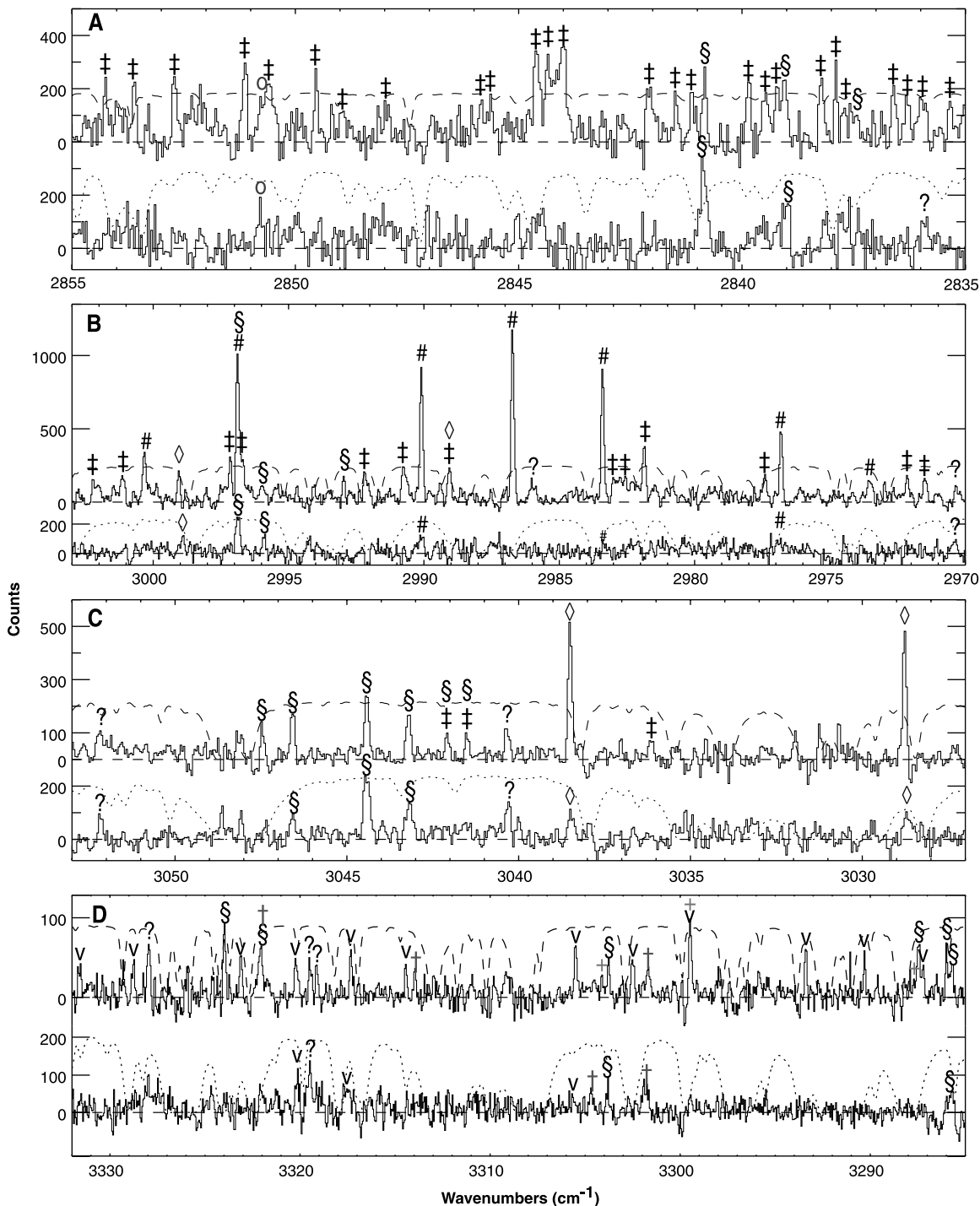
R0. (**D**) Setting KL2, order 25. Hydrogen cyanide and acetylene region. Marked lines in comet Lee include the following. v: HCN, ν_3, (13 lines); §: OH (1-0) and (2-1); and +: C_2H_2, ν_3, R3, and P5. Only HCN, NH_2 (†), and OH are seen in C/LINEAR.

Lee (*70*) (Table 2). CH₃OH and HCN have similar volatility, so they should be depleted by similar factors in C/LINEAR as compared with other OC comets, if temperature was a controlling factor. But CH₃OH is much more strongly depleted than HCN. Our upper limit for CH₃OH (<0.17% of H₂O) is lower than even the smallest abundance measured for any other OC comet to date; these exhibit a wide range in CH₃OH abundance, ∼ 0.5 to 5% relative to water (*7*, *8*). Our four comparative OC comets fall toward the low end of that range: Lee = 1.4 ± 0.3% (*10*), Halley = 1.7 ± 0.04 % (*71*), Hyakutake = 1.7% (*43*), and Hale-Bopp = ∼2% (*72*). The severe depletion of methanol in C/LINEAR, in the presence of a mild depletion of HCN but normal H₂S/HCN and H₂CO/HCN, is difficult to explain on the basis of preferential sublimation or condensation fractionation. Chemical processing before accumulation may provide the simplest explanation.

Chemical alteration of precometary ices could result from a number of poorly constrained processes, such as partial vaporization of icy grain mantles during nebular infall, condensation fractionation of nebular gas, thermal processing of ices, and photochemical processing of ices and gas by energetic radiation [ultraviolet (UV) and x-rays]. In regions of high H-atom density (for example, induced by x-rays from the young Sun), icy grain mantles may have been efficiently hydrogenated, converting condensed-phase CO to CH₃OH and C₂H₂ to C₂H₆, whereas enhanced ion densities (mainly H₃⁺) may drive a rich gas-phase ion-molecule chemistry similar to that in dense cloud cores. Such processing could have enforced corresponding differences in the volatile (icy) and re-

Table 1. Observing log for C/LINEAR. R is the heliocentric distance, Δ is the geocentric distance, Δ-dot is the geocentric velocity, and RP is the resolving power ($\lambda/\delta\lambda$).

UT date (July 2000)	R (AU)	Δ (AU)	Δ-dot (km/s)	RP ($\lambda/\delta\lambda$)	Setting (cm⁻¹)	Targets	On source time (min)
3.70–3.75	0.886	0.905	−63.6	24,000*	2149.5	CO, H₂O	24
4.56–4.59	0.877	0.868	−63.5	″	2981.5	C₂H₆, CH₃OH	28
4.59–4.61				″	2138.0	CO, H₂O	24
4.62–4.65				″	2149.5	CO, H₂O	24
4.71–4.78				12,000*	2976.0	CH₄, C₂H₆	48
4.78–4.86				″	3307.2	HCN, C₂H₂	24
5.57–5.63	0.868	0.832	−63.4	24,000*	2981.5	C₂H₆, CH₃OH	76
5.63–5.64				″	3041.0	CH₄ R1, OH	8
5.64–5.73				12,000*	3041.0	CH₄ R1, OH	60
5.76–5.84				″	2149.5	CO, H₂O	48
9.60–9.61	0.831	0.680	−61.0	15,000†	KL1	C₂H₆, CH₃OH, CH₄, OH	6
13.55–13.58	0.807	0.553	−54.9	15,000†	KL1	C₂H₆, CH₃OH, CH₄, OH	24
13.58–13.60				″	KL2	CH₄, C₂H₂, HCN, OH	28
13.62–13.63				″	K1	H₂O	16
13.63–13.64				″	M1	CO, H₂O	2

*CSHELL spectra (3 to 5 July) were acquired with either the 1″-wide slit (RP ∼ 24,000) or the 2″-wide slit (RP ∼ 12,000).   †NIRSPEC spectra (9 and 13 July) were acquired with the five-pixel-wide slit (0.72″ × 24″ on the sky).

Table 2. Parent volatiles in C/LINEAR.

Species	Date (July 2000)	Line identification	g_1* 10⁻⁵ ph s⁻¹ per molecule	Production rate 10²⁶ s⁻¹	Abundance H₂O = 100 C/LINEAR†	Abundance H₂O = 100 Comparison comets‡
H₂O	3.72	1₁₁–1₁₀§	0.0573	200 ± 60		
	4.60	0₀₀–1₀₁§	0.0953	230 ± 50		
	4.63	1₁₁–1₁₀	0.0573	210 ± 110		
	5.68	OH‖	0.0044	510 ± 110		
	5.80	1₁₁–1₁₀	0.0573	746 ± 74		
	9.6	OH¶	0.011	320 ± 70		
	13.58	OH‖	0.010	730 ± 50		
	13.63	1₁₁–1₁₀, 0₀₀–1₀₁	0.1526	446 ± 72		
CO 1-0	4.60	R0, R1, P1, P2	6.71	<4.2#	<1.9**	
	5.80	R1	1.90	7.0 ± 2.0	0.94 ± 0.27	1.8–12
	13.63	R1–R4, P3	10.2	2.0 ± 1.5	0.45 ± 0.34	
CH₄ ν_3	5.70	R1	3.0	0.59 ± 0.13	0.09 ± 0.02	
	13.58	R1	3.0	0.95 ± 0.14	0.15 ± 0.02	0.7
	13.58	R0	3.65††	0.90 ± 0.28	0.14 ± 0.04	
C₂H₆ ν_7	4.58	ᴾQ₁ + ᴾQ₂	7.81	<0.68	<0.30	
	5.60	ᴾQ₁ + ᴾQ₂	7.81	<0.56	<0.08	
	9.6	ᴿQ₁, ᴾQ₁, ᴾQ₂, ᴾQ₃	13.7	<0.24	<0.08	
	13.58	ᴿQ₁	3.47	0.80 ± 0.12	0.13 ± 0.02	0.6
	13.58	ᴿQ₁, ᴾQ₃	5.84	0.83 ± 0.14	0.13 ± 0.02	
C₂H₂ ν_3	13.58	R3	1.7	<0.89	<0.14	0.3
CH₃OH	13.58	ν_3, Q branch	1.4‡‡	<1.1	<0.17	1.7
HCN ν_3	13.58	R1, R2, P2	8.0	0.61 ± 0.17	0.10 ± 0.03	0.2–0.4

*The rotational temperature was assumed to be 50 K for all species other than OH.   †The production rate of water (in units of 10²⁶ s⁻¹) is taken to be 227 ± 60 on UT 4 July, 672 ± 66 on UT 5 July, and 638 ± 44 on UT 13 July.   ‡The mean value for Halley, Hyakutake, Hale-Bopp, and Lee is given unless individual values vary greatly; then the range is given.   §These are lines of the ν_3-ν_2 band of H₂O, detected directly.   ‖These data refer to the OH line group near 3046 cm⁻¹, consisting of emission from v' = 1, J' = 10.5 2⁺ and 2⁻ and J' = 11.5 1⁻ and 1⁺. Only the P12.5 1⁻ (J' = 11.5 1⁻) line fell within the CSHELL pass-band on 5.7 July (Fig. 1C). On 13.58 July, three lines were detected; the J' = 10.5 2⁺ line was extinguished by terrestrial water vapor (Fig. 2C). The tabulated g factors assume a prompt emission mechanism.   ¶These data refer to intensities measured for the OH line group near 2996 cm⁻¹, consisting of emission from v' = 1, J' = 12.5 2⁺ and 2⁻. The tabulated g factors assume a prompt emission mechanism.   #Upper limits correspond to the 2σ (95% confidence) level. Errors are based on stochastic noise only.   **Guiding and seeing can cause systematic errors in nucleus-centered production rates; however, our approach for determining global production rates mitigates these effects (*47*). Moreover, when two species are measured simultaneously (such as CO and H₂O), the ratio of their production rates is even more secure than the individual Qs. For this reason, we base the CO mixing ratio on the H₂O production rate measured simultaneously with CO. Mixing ratios for CH₄, C₂H₆, C₂H₂, CH₃OH, and HCN for each date are based on the weighted average of Q_{H_2O} retrieved from H₂O and OH emissions on that date. This approach guards against erroneous mixing ratios that might otherwise arise when global Qs are derived (*47*) from small-beam observations acquired during outbursts.   ††After (*46*).   ‡‡The modeled fluorescence efficiency was convolved with the atmospheric transmittance to arrive at an effective g factor.

fractory organic fractions in comets, as nebular conditions changed with heliocentric distance and/or with time.

Some interstellar material is expected to survive in the inner giant planets' region. Examples include amorphous (interstellar) silicate grains and low-temperature refractory organics (including polymers such as polyoxymethylene), and these would be carried into precometary grains unscathed, along with material modified in the nebula. The surviving organic grains could serve as precursors of H_2CO and HCN. In models of "hot cores" of molecular clouds, HCN and H_2S survive after ~10^4 years, whereas CH_3OH is rapidly destroyed by gas-phase chemistry (73, 74). We might expect to find HCN, H_2S, and H_2CO in recondensed precometary ices, whereas methanol is depleted by gas-phase chemical reactions, and the specific abundance of CO, methane, ethane, and acetylene are controlled by condensation of nebular gases with water (67). The unusual chemistry of ices in C/LINEAR is preliminarily consistent with this view.

Oort cloud comets may also contain some processed material from the terrestrial planets' region, in relative abundances decreasing with distance from the young Sun. Nebular turbulence can transport material from the terrestrial planets' region outward about as far as Uranus (75), leading to major reductions (from interstellar values) in the ratio of recondensed HDO/H_2O in re-formed precometary ices (76) and coincidental inclusion of crystallized silicates (77, 78). In this picture, the enriched D/H ratio in comets Halley, Hyakutake, and Hale-Bopp is indicative of interstellar ice (79, 80), but the D/H ratio would be lower in comets formed near Jupiter and Saturn. The low D/H ratio in Earth's oceans could reflect the contribution of Jovian-class (81) comets (82, 83), which would have delivered most of the mass. If C/LINEAR is one such comet, its unusual organic composition may require reevaluation of the delivery of prebiotic organic material delivered to the young Earth by comets.

References and Notes

1. M. J. Mumma, P. R Weissman, S. A. Stern, in *Protostars and Planets III* (Univ. of Arizona Press, Tucson, AZ, 1993), pp. 1177–1252.
2. W. M. Irvine, F. P. Schloerb, J. Crovisier, B. Fegley, M. J. Mumma, in *Protostars and Planets IV* (Univ. of Arizona Press, Tucson, AZ, 2000), pp. 1159–1200.
3. The orbits of Oort cloud comets display the dynamical Tisserand invariant $T_i < 2$. They include Halley-type orbits, long-period comets, and dynamically new comets.
4. Temperatures are approximate. They depend on the degree of nebular clearing, the luminosity of the young Sun, and other details (1).
5. L. Dones *et al.*, *Bull. Am. Astron. Soc.* **32**, 1060 (2000).
6. Roughly half of the comets remaining in the Oort cloud after 4 gigayears originated in the region from 5 to 30 AU; the remainder originated beyond 30 AU (5). Chemical differences among Oort cloud comets are revealed when parent volatiles are studied directly; for example, methanol varies from 0.5 to 7% (7, 8) whereas native CO varies from 1.8 to 12% (9, 10). However, until

recently too few parent volatiles were measured to permit inferences regarding origins. Studies of destruction products such as C_2 and CN have revealed differences among Jupiter-family comets, and to a much lesser degree among Oort cloud comets (11). The reason for this difference is not fully understood.
7. M. J. Mumma, in *From Stardust to Planetesimals: Review Papers* (Astronomical Society Pacific Conference Series 122, San Francisco, CA, 1997), pp. 369–396.
8. D. Bockelée-Morvan, T. Y. Brooke, J. Crovisier, *Icarus* **116**, 18 (1995).
9. M. A. DiSanti *et al.*, *Nature* **399**, 662 (1999).
10. M. J. Mumma *et al.*, *Astrophys. J.* **546**, 1183 (2001).
11. M. F A'Hearn *et al.*, *Icarus* **118**, 223 (1995).
12. The International Astronomical Union (IAU) designations of the four comparison comets are: 1P/Halley, C/1996 B2 (Hyakutake), C/1995 O1 (Hale-Bopp), and C/1999 H1 (Lee).
13. M. J. Mumma, *Nature* **383**, 581 (1996).
14. J. Crovisier, *Earth Moon Planets* **79**, 125 (1999).
15. D. Bockelée-Morvan *et al.*, *Astron. Astrophys.* **353**, 1101 (2000).
16. R. Meier, T. C. Owen, *Space Sci. Rev.* **90**, 33 (1999).
17. J. Crovisier *et al.*, *Science* **275**, 1904 (1997).
18. M. J. Mumma, *Infrared Phys.* **29**, 167 (1989).
19. M. J. Mumma *et al. Astron. Astrophys.* **187**, 419 (1987).
20. V. A. Krasnopolsky *et al.*, *Science* **277**, 1488 (1997).
21. V. A. Krasnopolsky, M. J. Mumma, *Astrophys. J.* **549**, 629 (2001).
22. S. A. Stern *et al. Astrophys. J.* **544**, L169 (2000).
23. G. H. Stokes *et al.*, *Icarus* **148**, 21 (2000).
24. B. Marsden, personal communication.
25. M. J. Mumma *et al.*, *Science* **272**, 1310 (1996).
26. T. Y. Brooke *et al.*, *Nature* **383**, 606 (1996).
27. M. A. DiSanti *et al.*, *Bull. Am. Astron. Soc.* **32**, 1071 (2000).
28. N. Dello Russo *et al.*, *Icarus* **135**, 377 (1998).
29. K. Magee-Sauer *et al.*, *Icarus* **142**, 498 (1999).
30. N. Dello Russo *et al.*, *Icarus* **143**, 324 (2000).
31. We used the IRTF's CSHELL (32).
32. T. P. Greene *et al.*, in *Proc. SPIE* **1946**, 311 (1993).
33. We used the Keck Observatory's NIRSPEC (34).
34. I. S. McLean *et al.*, in *Infrared Detector Arrays for Astronomy* (SPIE Conference Proceedings 3354, Bellingham, WA, 1998), pp. 566–578.
35. CSHELL affords a relatively small spectral grasp for each grating setting, so several separate instrument settings are needed to provide adequate spectral coverage for a typical molecular vibrational band. The 1K-by-1K detector array in NIRSPEC provides a larger spectral grasp for each order and the echelle grating is cross-dispersed, permitting multiple spectral orders to be sampled simultaneously. The instantaneous spectral coverage in the organics region (3.4 μm) is thus about 24 times larger for NIRSPEC than for CSHELL.
36. The slit was oriented east-west on the sky for all observations reported in this paper. Cometary spectra were acquired using sequences of four scans (switching between the A and B beams in a sequence of ABBA and keeping the comet on-slit for each position) with a total integration time of 4 min on-source per sequence (the K1 setting used 8 min per sequence). With CSHELL, the slit length was 30 arc-sec (150 detector rows) on the sky, and the telescope was nodded 15 arc-sec. We used the 2-arc-sec-wide slit and guided with the internal camera until sunrise. Thereafter, we imaged after each spectral sequence (in the ABBA sequence) to correct tracking and guiding. For NIRSPEC, the slit length was 24 arc-sec (~125 detector rows) on the sky, and the telescope was nodded 12 arc-sec. During K- and L-band observations with NIRSPEC, guiding was accomplished with the internal camera (SCAM) with the KL filter.
37. For each grating setting, spectra of IR standard stars were acquired for absolute flux calibration of the comet spectra. Stellar spectra were acquired with the same slit width used for the comet, and slit losses were estimated by assuming an azimuthally symmetric stellar profile. Appropriate corrections were incorporated into the absolute flux calibrations.
38. Initial data processing included removal of high dark current pixels and cosmic ray hits using median- and

sigma-filtering, and registration of spectral frames. The raw spatial-spectral frames are usually anamorphic in both spectral and spatial directions. We resampled the frames, straightening the A and B beams independently within each order so that the spectral dimension fell along a row and the spatial dimension was orthogonal to this. This process also adjusts the spectral dispersion to a common value, row by row. Spectra were then extracted by summing seven rows about the center of each beam position, and those spectra were combined.
39. Atmospheric transmittance models were calculated with the Spectrum Synthesis Program (SSP), which accesses the HITRAN-1992 Molecular Data Base. SSP models were used to assign wavelength scales to the spectra and to establish absolute column burdens for relevant absorbing species in the terrestrial atmosphere. The transmittance model was binned to the instrumental sampling interval, convolved to the resolution of the comet spectrum, and normalized to the cometary continuum. For additional details on our data processing techniques, see (9, 28).
40. Rotational temperatures should differ for individual species when radiative cooling controls rotational populations. However, the temperatures retrieved for CO, HCN, and C_2H_6 in comet Lee agree quite well, which may reflect control of rotational populations by electron collisions in the inner coma (41, 42). We therefore adopt a common temperature (50 K) for all species in C/LINEAR.
41. X. Xie, M. J. Mumma, *Astrophys. J.* **386**, 720 (1992).
42. D. Bockelée-Morvan *et al.*, *Planet. Space Sci.* **42**, 665 (1994).
43. N. D. Biver *et al.*, *Astron. J.* **118**, 1850 (1999).
44. M. J. Mumma *et al.*, *Astrophys. J.* **531**, L155 (2000).
45. N. Dello Russo *et al.*, in preparation.
46. T. Y. Brooke *et al.*, *Astrophys. J.* **372**, L113 (1991).
47. For bright comets, we measure the trend of these "spherical" production rates versus distance from the nucleus (along the slit) and form a "symmetric" Q from the east-west mean at each offset position. The nucleus-centered extract is invariably too small (due to slit losses caused primarily by seeing), but off-nucleus extracts of the symmetric Q are less affected and they quickly reach a terminal value [unless a distributed source is also present (9)]. This terminal value is taken to be the "global" production rate. For C/LINEAR, we measured the global production rate and its growth from the nucleus-centered value for H_2O, CH_4, and OH; growth factors were measured for these species, and (in all frames) for dust. We used those growth factors to scale nucleus-centered production rates for other species (HCN, C_2H_2, C_2H_6, CH_3OH, and OH) (Table 2).
48. Dissociative excitation of H_2O creates OH fragments in rotationally and vibrationally excited states (49–51). The newly formed OH promptly radiates a vibrational quantum (within a few milliseconds) and the rotational distribution then cools to ambient temperatures through collisions; hence, subsequent fluorescent or collisional excitation of the observed lines is negligible (52). The excitation efficiency (g factor) for OH prompt emission is determined by the solar UV flux (mainly Lyman-alpha) responsible for dissociative excitation of water and by the quantum structure of the water molecule. The relative line intensities within each OH quadruplet depend only on the dissociative quantum states of water itself, and so they are independent of the water production rate. They are also independent of the rotational temperature for water, to first order. Such high-J lines cannot be excited by fluorescent pumping (either UV or IR) of thermalized OH in the coma.
49. T. Carrington, *J. Chem. Phys.* **41**, 2012 (1964).
50. I. Yamashita, *J. Phys. Soc. Jpn.* **39**, 205 (1975).
51. P. Andresen *et al.*, *J. Chem. Phys.* **80**, 2548 (1984).
52. J. Crovisier, *Astron. Astrophys.* **213**, 459 (1989).
53. The analysis of methanol emission depends on the availability of quantum band models that can be tailored to the low rotational temperatures typical of comets (30 to 100 K) (44). These models exist (54, 55) for the ν_3 vibrational band centered near 2844 cm^{-1}, but they are only now being developed for ν_2 and ν_9 (56). For this reason, we targeted the ν_3 band in order 22 when selecting the setting KL1. We tailored the ν_3

quantum band model (55) to 50 K and used it to obtain a g factor for the Q-branch region and an upper limit to the CH₃OH production rate.

54. R. H. Hunt *et al.*, *J. Mol. Spectrosc.* **149**, 252 (1991).
55. D. C. Reuter, *Astrophys. J.* **386**, 330 (1992).
56. Li-H. Xu *et al.*, *J. Mol. Spectrosc.* **185**, 158 (1997).
57. We tailored our ethane fluorescence model (45) to 50 K rotational temperature.
58. T. L. Farnham *et al.* *Science* **292**, 1348 (2001).
59. H. A. Weaver *et al.* *Science* **292**, 1329 (2001).
60. D. Bockelée -Morvan *et al.*, *Science* **292**, 1339 (2001).
61. The water production rate reported by (59) may need downward revision, if OH electronic prompt emission is significant (62). HST fluxes show a continual decrease from July 6.74 to July 6.87, so the peak production apparently occurred before July 6.74 (59).
62. S. A. Budzien, P. D. Feldman, *Icarus* **90**, 308 (1991).
63. J. T. T. Mäkinen *et al.*, *Science* **292**, 1326 (2001).
64. P. Eberhardt *et al.*, *Space Sci. Rev.* **90**, 45 (1999).
65. The CO mixing ratio reported by (25) is being revised upward because of optical depth effects (27) and improvements in our data processing techniques (47).
66. Our upper limit obtained for C₂H₂ shows that it is less abundant in C/LINEAR than in the four comparison comets; for example, in Lee C₂H₂/H₂O = 0.27 ± 0.03 and in Hale-Bopp C₂H₂/H₂O = 0.31 ± 0.1% (10).
67. G. Notesco, A. Bar-nun, *Icarus* **122**, 118 (1996).
68. G. Notesco *et al.*, *Icarus* **125**, 471 (1997).
69. K. R. Lang, *Astrophysical Quantities* (Springer, Berlin, 1980), p. 162.
70. Bockelée-Morvan *et al.* (60) assumed the mixing ratio (HCN/H₂O) to be 0.1% in C/LINEAR. Radio measurements generally show cometary HCN/H₂O ~ 0.1% (15), but IR measurements show differences among comets. For example, on 13.8 July, HCN in C/LINEAR (~ 0.10 ± 0.03) was less than that in comets Lee (0.23 ± 0.02%) and Hale-Bopp (0.40 ± 0.05%) (10, 29). Differences between radio and IR measurements are not understood at present. The CN/OH ratio is also low in C/LINEAR (58), as compared with comets Halley, Hyakutake, and Hale-Bopp. However, NH/OH is normal (58), as are our NH₂/OH line intensities (Fig. 2D).
71. P. Eberhardt *et al.*, *Astron. Astrophys.* **288**, 315 (1994).
72. D. Despois *et al.*, *Earth Moon Planets* **79**, 103 (1999).
73. J. Hatchell *et al.*, *Astrophys. J.* **338**, 713 (1998).
74. S. B. Charnley *et al.*, *Astrophys. J.* **399**, L71 (1992).
75. A. Drouart *et al.*, *Icarus* **140**, 129 (1999).
76. O. Mousis *et al.*, *Icarus* **148**, 513 (2000).
77. J. Nuth *et al.*, *Nature* **406**, 275 (2000).
78. D. Bockelée-Morvan *et al.*, *Bull. Am. Astron. Soc.* **32**, 1081 (2000).
79. Recent models of gas phase chemistry in the protoplanetary disk have reproduced the deuterium enrichment seen in HCN and H₂O in Hale-Bopp (80).
80. Y. Aikawa, E. Herbst, *Astrophys. J.* **526**, 314 (1999).
81. We use the term "Jovian-class" to mean a comet that formed in the Jupiter-Saturn nebular region. This should not be confused with the term "Jupiter-family" comet. The Jupiter-family comets are a dynamical grouping with Tisserand invariant 2 < T_i < 3; they formed over a much wider range of heliocentric distance (from the Kuiper belt inward) and only later entered their present orbits.
82. A. Delsemme, *Planet. Space Sci.* **47**, 125 (1998).
83. A. Delsemme, *Icarus* **146**, 313 (2000).
84. Supported by the NASA Planetary Astronomy Program (grants RTOP 344-32-30-07 to M.J.M. and NAG5-7905 to M.A.D.), by the NASA Planetary Atmospheres Program (grant NAG5-7753 to N.D.R.), and by NSF (grant AST-9619461 to K.M.S.). The NASA IRTF is operated by the University of Hawaii under contract to NASA. The Keck Observatory was made possible by the generous financial support of the W. M. Keck Foundation; it is operated as a scientific partnership among the California Institute of Technology, the University of California, and NASA. We thank the staff of IRTF and Keck for their expert assistance and H. Levison for valuable discussions. M.J.M. thanks S. T. Mumma and S. E. Selonick, without whose support this research would not have been possible.

Outgassing Behavior and Composition of Comet C/1999 S4 (LINEAR) During Its Disruption

Dominique Bockelée-Morvan,[1] Nicolas Biver,[1] Raphaël Moreno,[2] Pierre Colom,[1] Jacques Crovisier,[1] Éric Gérard,[1] Florence Henry,[1] Dariusz C. Lis,[3] Henry Matthews,[4] H. A. Weaver,[5] Maria Womack,[6] Michel C. Festou[7]

The gas activity of comet C/1999 S4 (LINEAR) was monitored at radio wavelengths during its disruption. A runaway fragmentation of the nucleus may have begun around 18 July 2000 and proceeded until 23 July. The mass in small icy debris (≤30-centimeter radius) was comparable to the mass in the large fragments seen in optical images. The mass budget after breakup suggests a small nucleus (~100- to 300-meter radius) that had been losing debris for weeks. The HNC, H₂CO, H₂S, and CS abundances relative to H₂O measured during breakup are consistent with those obtained in other comets. However, a deficiency in CH₃OH and CO is observed.

Cometary nuclei are porous bodies containing ices and refractory material. It is not uncommon for cometary nuclei to split into several fragments (1, 2), which demonstrates their fragile nature. In addition, a number of comets have been observed to disappear catastrophically (3), which suggests their disintegration into small debris being stripped of their ices on short time scales. Owing to the unpredictable nature of such events, data on the evolution of the gaseous activity of a cometary nucleus undergoing disruption are sparse. So far, gas monitoring observations of a fragmenting comet were only obtained for 73P/Schwassmann-Wachmann 3 (4).

Comet C/LINEAR's close approach to Earth at 0.374 astronomical units (AU; 1 AU = 1.496 × 10¹¹ m is the average Earth-Sun distance), just a few days before perihelion on 26 July 2000, when the comet was 0.765 AU from the Sun, together with favorable brightness predictions, made this comet a suitable target for spectroscopic observations at radio wavelengths. This spectral range allows the study of many volatile molecular species released by the nucleus as it approaches the Sun (5–9). Radio observations of C/LINEAR were planned to expand our data sample used for comparative studies of cometary composition. Serendipitously, they provided unprecedented data on the outgassing behavior of a nucleus undergoing almost complete disruption.

The observations were made with five different radio telescopes. OH 18-cm observations were scheduled from 6 July to 3 August 2000 at the Nançay radio telescope, upgraded with a new focus system (10). These observations were aimed at providing the production rate of water, which is the source of the OH radical and the most abundant constituent of cometary ices. Observations in the millimeter and submillimeter ranges were performed with the National Radio Astronomy Observatory (NRAO) 12-m Kitt Peak telescope, the Caltech Submillimeter Observatory (CSO, 10.4 m), the James Clerk Maxwell Telescope (JCMT, 15 m), and the Institut de Radio Astronomie Millimétrique (IRAM) 30-m telescope. Data were acquired in early January 2000, when comet C/LINEAR was still at the distance r_h = 3.2 AU from the Sun, on 17 to 20 June 2000 (r_h = 1.0 AU), 1 July (r_h = 0.9 AU), and almost daily around perihelion from 18 July to 3 August (r_h ~ 0.77 AU). Seven molecular species were searched for (HCN, HNC, CO, H₂CO, CH₃OH, H₂S, and CS), some of them through several rotational transitions (Table 1). All species, except CO and CH₃OH, were detected (Figs. 1 and 2). In contrast to other species, which were observed only on selected dates, HCN was continuously monitored during the scheduled observing periods (Table 1).

The observed line intensities were converted into gas production rates with standard techniques (7, 11–13). In a normally behaved comet, one would expect the outgassing rates to follow a rather smooth r_h^{-n} law, with n ranging from 2 to 4. However, observations of the HCN, H₂O (14), OH (15, 16) (Fig. 3),

¹Observatoire de Paris-Meudon, F-92195, Meudon, France. ²Institut de Radioastronomie Millimétrique, 300 rue de la Piscine, Domaine Universitaire, F-38406, St. Martin d'Hères Cedex, France. ³Department of Physics, California Institute of Technology, MS 320-47, Pasadena, CA 91125, USA. ⁴Joint Astronomy Centre, 660 North A'ohoku Place, Hilo, HI 96720, USA. ⁵Johns Hopkins University, 3400 North Charles Street, Baltimore, MD 21218–2686, USA. ⁶St. Cloud State University, 720 Fourth Avenue S, MS 324, St. Cloud, MN 56301– 4498, USA. ⁷Observatoire Midi-Pyrénées, 14 avenue Edouard Belin, F-31400, Toulouse, France.